IEEE Transactions on Nuclear Science, Vol. NS-27, No. 1, February 1980

DESIGN CRITERIA FOR MULTI-SLICE POSITRON EMISSION-COMPUTED TOMOGRAPHY DETECTOR SYSTEMS

L.R. Carroll, G.O. Hendry, J.D. Currin
The Cyclotron Corporation
Berkeley, California

Abstract

Design criteria for single-slice positron emission computed tomography systems have been extensively discussed in the literature. We wish to extend the current methodology and suggest some additional tools for optimizing the design of multi-slice tomographic systems.

Practical results using Bismuth Germanate coincidence detectors are shown. The effect of shielding design on overall system performance is evaluated with the help of a simple graphical technique.

Introduction

The study-time required to obtain an image using positron emission-computed tomography depends on statistical requirements; the desired precision of the measurement, the source distribution, the number of quantitation cells in the image histogram, and other factors relating to attenuation correction and contamination from unwanted background.

Several authors have reported on statistical requirements in positron computed tomography. Concise formulas and useful examples are developed in Reference 1 and 2. In order to relate such examples to practical imaging instruments, we shall review some properties of circular-ring positron coincidence detector systems.

Detector Properties

Following the introduction of Bismuth Germanate (BGO) as a potential scintillation detector for positron cameras by Cho and Farukhi (3) and the successful implementation of a BGO tomograph by Thompson, et al (4), this material is coming into wide use, replacing sodium iodide in applications involving positron annihilation coincidence detection.

Some representative timing and energy spectra for a detector pair using 2 cm diameter x 3.8 cm long BGO crystals (purchased from Harshaw Chemical Co.) coupled to 3/4" photomultiplier tubes (Amperex type PM 1910) are shown in Figures 1a and 1b.

The measurements were conducted in air, without any scattering medium around the source (^{22}Na), nor any shielding around the crystals. The time discriminator is of the leading edge type, of our own design. The timing spectrum, Figure 1a, includes only events which exceed a 300 KeV lower threshold.

Figure 1b shows two energy spectra; a "singles" spectrum superimposed upon a pulse-height spectrum gated by the coincidence detector. Note the absence in the latter of the high-energy (1022 KeV) peak and the reduced low-energy component which would be present due to scatter from the work-bench and test setup. The 300 KeV lower threshold is also quite obvious.

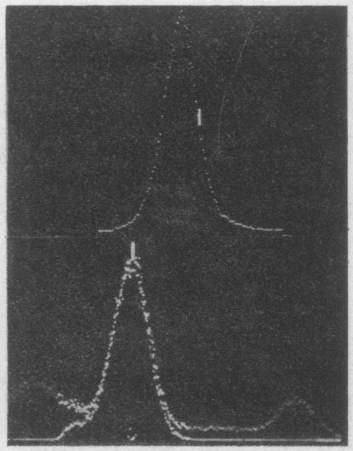

FIG. 1a
BGO TIMING SPECTRUM. EACH CHANNEL CORRESPONDS TO 250 PS.

FIG. 1b
BGO ENERGY SPECTRUM WITH AND WITHOUT COINCIDENCE GATING, USING ^{22}Na SOURCE.

In this experiment the (FWHM) and (FWTM) timing spread was 5 and 10.5 NS respectively, while the FWHM energy spread was 22% at 511 KeV.

The intrinsic (scatter-free) coincidence-gated pulse-height spectrum for BGO has a very high photo fraction. As reported in (3) we can profitably employ energy selection to discriminate against wide-angle and multiple-scattered photons without reducing the response to unscattered photons.

Ideally, we should set a narrow timing window and a high energy threshold to reduce random and scatter background. However, it can be quite difficult to maintain stable, uniform response among a large ensemble of scintillation detectors when energy and timing windows are too tight with respect to individual detector characteristics.

Small gain drifts can cause time-varying responses which cannot be corrected by pre- or post- study calibration techniques. These variations introduce systematic artifacts which can be considerably more troublesome than purely random noise due to counting statistics.

A prudent approach to system design allows sufficient margin for variations among components, and some allowance for drift with time and temperature.

Moreover, in the discussion to follow, it is our intention to focus on detector and shielding geometry, so that we will fix a number of parameters related to individual detectors. In accordance with the above, and in the light of known performance properties as shown in Figure 1, we shall assume the following:

Coincidence pair efficiency, $E^2 = .5$

Lower energy (Pulse-height) threshold - 300 KeV

Coincidence timing window ($2\tau r$) = 20 NS

0018-9499/80/0200-0485$00.75

These fixed parameters are factored into formulas given in Reference 5 and appear as constant coefficients in formulas presented here.

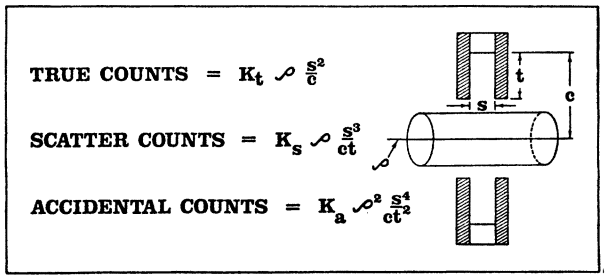

FIG. 2 PHANTOM MODEL

Sensitivity

The phantom model to be discussed is a long 20 cm diameter water-filled vessel with activity concentrated on the axis. Following the methodology established in Reference 5, the geometry of Figure 2 for a single slice, and factoring in the fixed parameters established above, we have:

$$(1)\quad C_t = \frac{670\,\rho\,S^2P^2}{c} \text{ counts/second}$$

Where

- C_t = count rate for true, unscattered events
- ρ = activity concentration in μCi/axial cm
- S = detector gap width (axial)
- P = detector packing factor: 1.0 = fully packed
- C = ring radius

Scatter

For relatively coarse pulse-height analysis used with discrete, BGO-crystal positron coincidence detection systems, a primary defense against scatter is a reasonably large ring radius (small θ_f as designated in Reference 5).

For the present model; in a single slice:

$$(2)\quad C_b = \frac{2390\,\rho P^2 S^3}{cT} \text{ counts/sec}$$

where T = shield slit depth

Random Coincidences

Annihilation coincidence detection systems are subject to a perturbing background due to random, or accidental coincidences.

For this model the rate of accidental coincidences for a single slice is given by:

$$(3)\quad C_a = \frac{40\,\rho^2P^2S^4}{cT^2}$$

Count Rate Capability

Observe that C_a in Formula (3) increases as the square of activity concentration, ρ. At some point the rate of random background counts becomes so large as to introduce serious errors in the final image histogram, even though in principle we subtract this background contribution. We shall propose a criterion - admittedly arbitrary - wherein the maximum useable count rate is the rate at which true counts and random counts are equally abundant in the detector output data.

Accordingly, set C_t in equation (1) equal to C_a in equation (3) to find the activity concentration, ρ max, at which the rate for "trues" equals that for "randoms" in the detector field of view.

$$(4)\quad \rho \text{ max} = 16.75\,\frac{T^2}{S^2}$$

The count rate for true events at activity concentration ρ max is given by

$$(5)\quad \hat{C}_t = 1.12 \times 10^4\,\frac{T^2P^2}{c}$$

Deadtime

Deadtime in scintillation detectors and coninicidence electronics causes a loss of efficiency at high count rates. Also, dead time introduces a non-linear component which can upset quantitative measurements if it is not taken into account. Sources of deadtime include scintillator decay time, integration time for energy measurement, coincidence circuit busy time, address calculation, and computer access time. If we assume that the system is designed with sufficient redundancy and parallelism of channels, then we can estimate system live time fraction based on gross count rate per detector and estimated overall average "busy" time per incident photon.

Again, following Reference 5 and factoring in appropriate fixed parameters, for one slice:

$$(6)\quad \text{(System live fraction)} = \exp\,\frac{-.1\,\rho PS^2}{NT}$$

where N = number of crystals in a ring.

Effective Count Rate

We know that practical positron coincidence detector systems suffer from perturbing background. Therefore, evaluation of any system based on "sensitivity" alone is not adequate to predict statistical precision (6). Even if we could subtract a perfect estimate of the true mean background contribution, we would still have an excess noise contribution due to the variance of the observed counts.

Following a suggestion by Derenzo (7) we shall define an effective count rate.

$$(7)\quad Q(\rho) = \frac{(\text{trues rate})^2\,(\text{System live fraction})}{(\text{trues rate})+(\text{Scatter rate})+(\text{Random rate})}$$

All of these parameters can be evaluated given a knowledge of system geometry and equations (1) through (6). An example is given in Figure 3 of a plot of $Q(\rho)$ against activity concentration with various ring dimensions for a single slice tomograph, where the "patient" aperture has been fixed at 30 cm and the gap width, S, is fixed at 2 cm.

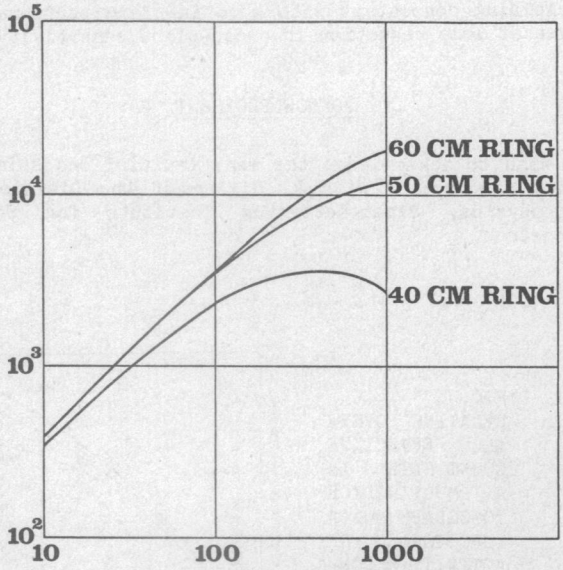

FIG. 3 EFFECTIVE COUNT RATE AS A FUNCTION OF ACTIVITY CONCENTRATION WITH DETECTOR DIAMETER AS PARAMETER

Multi-slice Systems

A multi-slice tomographic detector system can be assembled by stacking a number of single-slice ring detectors. In the absence of shielding septa between rings, the system sensitivity would grow as the square of the overall axial dimension. However, as pointed out earlier, for an extended phantom model the maximum useable system count rate, C_t, is governed by T^2/C - the square of shield depth divided by ring radius, and does not grow with S, the shield gap dimension.

Contemporary systems for positron annihilation coincidence detection feature modest timing and energy resolution. One may be tempted to improve sensitivity by increasing detector solid angle, but this may result in a rapid increase in random and scatter background.

The random contribution, in particular, may increase so markedly as to negate any advantage due to increased sensitivity. An effective strategy is to employ inter-ring septa which provide most of the benefits of good shielding, while maintaining the nearest-neighbor "cross-plane" slices.

Inter-ring Septa

The design of shielding septa has a substantial effect on overall performance of a multi-slice tomograph. In the complete absence of septa, nearest-neighbor cross-plane slices have twice the sensitivity of a straight-across slice. However, the ability to reject scatter and randoms is hopelessly degraded.

As the septa are made larger and larger (as a fraction of ring radius) the scatter and random rejection are improved while cross-plane sensitivity is diminished. Obviously, we would like to find the most satisfactory compromise.

Figure 4 suggests a graphical technique which aids in understanding the effect of septal "shadowing" on cross-plane sensitivity. Two detectors are subdivided into small segments. The ensemble of all possible rays joining the segments are drawn. The sensitivity is proportional to the weighted sum of rays joining the detectors that are not blocked by the septa. The axial point spread function can also be evaluated from the variation in ray density as a function of Z. Some computed results for straight (non-tapered) 3 mm tungsten septa betweeen 2 cm crystals in 60 cm diameter rings are given in Figure 5.

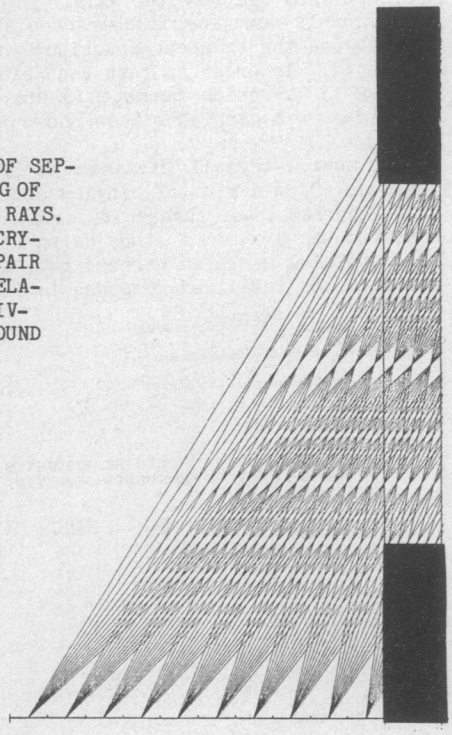

FIG. 4 EVALUATION OF SEPTAL SHADOWING OF CROSS-PLANE RAYS. ONLY ONE CRYSTAL OF THE PAIR IS SHOWN. RELATIVE SENSITIVITY IS FOUND BY COUNTING RAYS THAT ARE NOT BLOCKED BY SEPTA

The results reflect relative cross-plane sensitivity for a single crystal-pair and do not include the effect of reduced area packing factor when using round crystals. Nevertheless, when evaluating total system performance in a multi-slice tomograph, optimizing with respect to a total bulk of detector material, for a given spatial resolution in transverse planes, round crystals should be given careful consideration, even at a slight reduction in geometric packing factor.

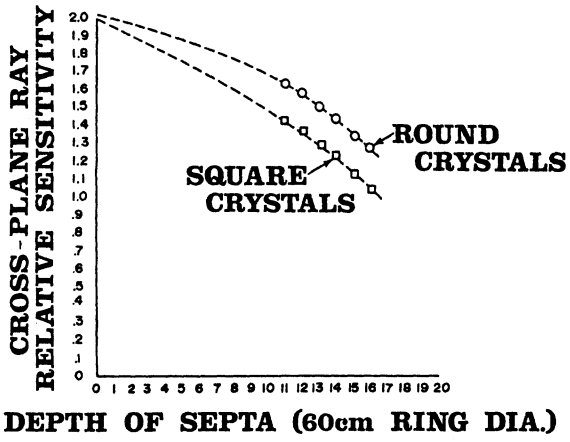

FIG. 5 CROSS-PLANE SENSITIVITY AS A FUNCTION OF SHIELD DEPTH FOR FIXED DETECTOR DIAMETER.

Shielding Effectiveness

The axial profile of point-source response in cross-plane slices varies substantially as a function of distance from the detector axis. In order to maintain a reasonably homogeneous characteristic it is necessary to use the thinnest practical inter-ring shielding septa. In order to test the shielding effectiveness of 3 mm thick tungsten septa, a simple bench experiment was carried out as shown in Figure 6.

For a source-crystal distance of 30 cm and shield depth of 13 cm a plot of singles counts in the photopeak (300 KeV lower threshold) as a function of source position was drawn. A study using 2-inch lead bricks for shielding was also carried out, and both are compared to the idealized response in Figure 7.

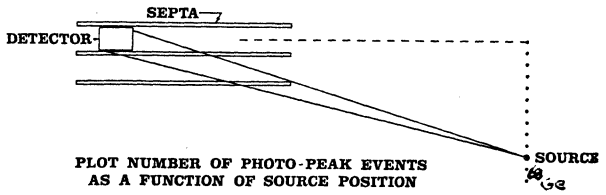

FIG. 6 BENCH EXPERIMENT

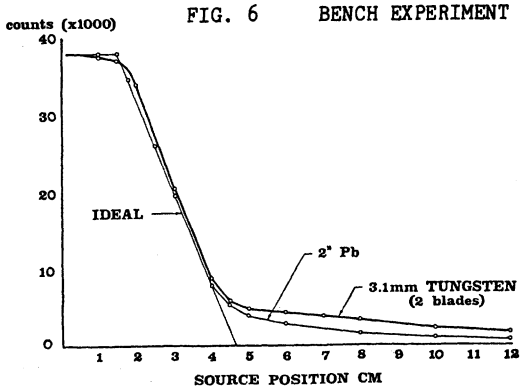

FIG. 7 RESPONSE FOR TUNGSTEN, LEAD, & IDEAL SHIELDING SEPTA

The integrated total counts for the lead-brick shielding is approximately 14% greater than the ideal, probably due to scatter off the bricks, while the 3 mm tungsten septa give 8% more single counts than the lead bricks due to penetration of the 511 KeV photons.

Overall Performance of Multi-slice Systems

Figure 8 summarizes the results of a calculation of overall effective countrate for a 5-layer (9-slice) tomograph of fixed 60 cm diameter and 2 cm gap width, with shielding depth as parameter. These results suggest overall effective countrate (as opposed to overall sensitivity) is optimized by employing inter-plane shielding consistent with good in-plane performance, even at some reduction in cross-plane sensitivity.

ACKNOWLEDGEMENT

I wish to acknowledge the many fruitful and stimulating discussions with R. Bigler of the Division of Biophysics, Sloan-Kettering Institute for Cancer Research.

FIG. 8 RELATIVE OVERALL EFFECTIVE COUNT RATE IN A MULTI-SLICE TOMOGRAPH AS A FUNCTION OF ACTIVITY CONCENTRATION, WITH SHIELD DEPTH AS PARAMETER.

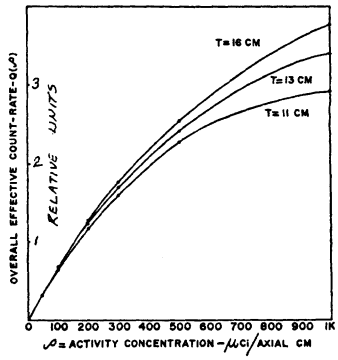

REFERENCES

1. Budinger, Derenzo, et al, "Emission Computer Assisted Tomography with Single Photon and Positron annihilation Photon Emitters", Journal of Computer Assisted Tomography. Vol 1, no. 1, Jan, 1977.

2. Budinger, et al, "Quantitative Potentials of Dynamic Emission Computed Tomography", Journal of Nuclear Medicine, Vol 19, No 3, March 1978.

3. Cho, Farukhi, "Bismuth Germanate as a potential Scintillation Detector in Positron Cameras". Journal of Nuclear Medicine. Vol 18 No 8, Aug 1977.

4. Thompson, Yamamoto, Meyer. Positome II: A High-efficiency Pet Device for Dynamic Studies (Abstract), Journal of Computer Assisted Tomography. Vol 2 No 5, Nov 1978.

5. Derenzo, Zaklad, Budinger, "Analytical Study of a High-Resolution Positron Ring Detector System for Transaxial Reconstruction Tomography" in Reconstruction Tomography in Diagnostic Radiology and Nuclear Medicine. Ter Pogossian, Phelps, Brownell, Cox, Davis, Evens, Editors. University Park Press, New York, Baltimore, 1977.

6. Phelps, Hoffman, Huang, Kuhl, Design Considerations in Positron Computed Tomography (PCT) IEEE Transactions on Nuclear Science, Vol NS-26 No. 2, April, 1979.

7. Derenzo, Optimization of Shielding in Positron Tomography Detector Systems. Presented at the Annual Meeting of the Society of Nuclear Medicine, Atlanta, June, 1979.